

few layers of gold to the ends of the molecule (see Fig. 2). A 'pyramid' of gold atoms at the surface is chosen to mimic a typical break junction and the lead cross-section is taken to be 3 by 3 layers of (111) gold. Six layers of gold are included, which is enough to converge the transmission. In the case of the thiol end group, the contacting geometry is taken to be the terminal sulphur binding to the top atom on the gold pyramid. The optimum binding geometry is found using DFT to minimize the gold-sulphur distance, which we find to be 2.5 Å.

A tight binding Hamiltonian describing this structure is then used to calculate the zero-bias transmission $T(E)$, where E is the energy of the incoming electron and the conductance is obtained via the Landauer formula $G(E) = G_0 T(E)$, where $G_0 = 2e^2/h$.

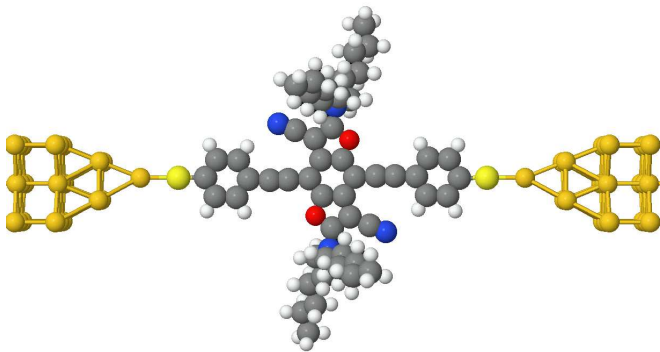


FIG. 2: Structure of the extended molecule **3**. Thiol anchor groups bind to top atom of the gold surface.

The results produced using this method usually do not agree with experimental measurements due to inherent problems associated with DFT, which inaccurately predicts the HOMO and LUMO eigenvalues. Consequently the resonances in $T(E)$ can appear at the wrong energies. In the literature, various corrections^{10,11} have been implemented to overcome this limitation. Here we present an alternative method which corrects both the HOMO-LUMO gap and also the energies of the HOMO-1 and LUMO+1 states. The method involves comparing the above DFT-based $T(E)$ with the transmission $T_M(E)$ of a model Hamiltonian H_M and then adjusting the parameters of the model such that model $T_M(E)$ coincides with DFT-based $T(E)$. More precisely, we adjust the model Hamiltonian parameters to minimize χ^2 , where

$$\chi^2 = \int_{E_1}^{E_2} (\log T(E) - \log T_M(E))^2 .$$

The choice of E_1 and E_2 is somewhat arbitrary and chosen to define an energy window containing two resonances below and two other above the Fermi energy. In practice, the fit does not depend strongly on this choice, provided there are no strong resonances too close to the limiting values on either side. Just like the DFT-based $T(E)$ the resonances of the model $T_M(E)$ will appear at the wrong energies. However, since the model Hamiltonian is known, it is now a simple matter to adjust the

model Hamiltonian parameters such that the resonances of $T_M(E)$ appear at the correct energies.

Since we are interested in correcting the the position of four frontier resonances (HOMO, LUMO, HOMO-1 and LUMO+1), we choose a four-state model Hamiltonian of the form:

$$H_M = \begin{pmatrix} 0 & \gamma_{11} & \gamma_{21} & \gamma_{31} & \gamma_{41} & 0 \\ \gamma_{11} & \epsilon_1 & \kappa_{12} & \kappa_{13} & \kappa_{14} & \gamma_{12} \\ \gamma_{21} & \kappa_{12} & \epsilon_2 & \kappa_{23} & \kappa_{24} & \gamma_{22} \\ \gamma_{31} & \kappa_{13} & \kappa_{23} & \epsilon_3 & \kappa_{34} & \gamma_{32} \\ \gamma_{41} & \kappa_{14} & \kappa_{24} & \kappa_{34} & \epsilon_4 & \gamma_{42} \\ 0 & \gamma_{12} & \gamma_{22} & \gamma_{32} & \gamma_{42} & 0 \end{pmatrix},$$

where ϵ_i is the energy of the state i , κ_{ij} describes the coupling between the molecular states i and j , and γ_{il} stands for the coupling between the molecular state i and the lead l , which can be the left one or right one. By decimating the Hamiltonian H_M and applying Dyson's equation, we obtain the surface Green's function G and the transmission probability $T_M(E) = |\nu G_{12}|^2$, where G_{12} is the off-diagonal element of G and ν is proportional to the group velocity in the identical leads.¹² This presents a fitting problem to the original DFT-based transmission function $T(E)$ with 18 free variables. The resulting fitted matrix elements of H_M can now be adjusted to yield resonances at the correct energies. Here we use wide-band approximation, in which ν is assumed to be energy independent. For molecule **3** shown in Fig. 2, a comparison between $T(E)$ and the uncorrected $T_M(E)$ is shown in Fig. 3. The corrected $T_M(E)$ for the same molecule can be seen in Fig. 7.

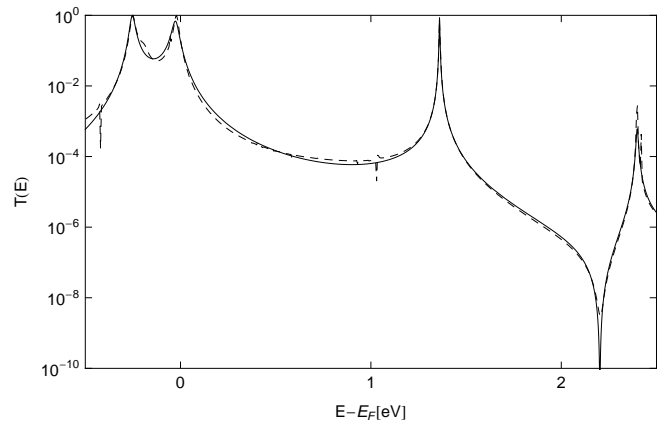


FIG. 3: The original DFT-based transmission function $T(E)$ (dashed line) and $T_M(E)$, the uncorrected transmission probability of the model Hamiltonian (solid line).

In principle, the correct resonance energies could be obtained experimentally. In the absence of experimental values, we obtain more accurate values for the frontier orbital energies using time-dependent DFT (TDDFT). In what follows, we use the numerical software NWChem¹³ with B3LYP¹⁴ exchange-correlation potential and 6-311G* basis functions. The overlap integrals

show that the lowest singlet excitation S_0 corresponds to the HOMO \rightarrow LUMO transition. Similar statements can be made with next few excitations and the HOMO \rightarrow LUMO+1 and HOMO-1 \rightarrow LUMO transitions. Using the first singlet excitation energy yields a good estimate for the positions of the resonant peaks around the Fermi energy, because this is the minimum energy required for the formation of a free electron-hole pair.¹⁵ In particular, when the Fermi energy is approximately in the middle of the HOMO-LUMO gap, the HOMO and the LUMO levels play equally important roles in the transport. Therefore the difference between their associated eigenenergies should be calculated when they are populated equally by one electron on each, which is given by the first singlet excitation. Two other excitations, corresponding to the HOMO \rightarrow LUMO+1 and HOMO-1 \rightarrow LUMO transitions are used to fix the HOMO-1 and LUMO+1 levels relative to the HOMO level.

So far we have discussed how to locate the relative positions of the resonant peaks around the Fermi energy, but we still have to fix the Fermi energy itself. To reliably locate the Fermi energy relative to the corrected resonance peaks, we shift the whole spectrum, so that the HOMO energy equals $E_F - IP_{\text{mol}}$, where IP_{mol} is the ionization potential of the molecule and $E_F = 5.1$ eV is the work function of gold.¹⁶ The ionization potential IP_{mol} is taken to be the difference between the total DFT energy of the neutral molecule, and that of the $+|e|$ -charged molecule, using the equilibrium geometry of the neutral molecule in both cases. This definition assumes that on the timescale of tunnelling transport, the molecule has no time to relax to the equilibrium geometry of the charged state, which would shift the corresponding eigenenergies around the Fermi level. To compute IP_{mol} , we again used NWChem with the same basis and exchange-correlation potential.

At this point, we have the corrected eigenenergies of the four states relative to the Fermi level, which we set to be the origin of energy. The correction of H_M is carried out by first diagonalizing the 4×4 molecular sub-matrix of H_M , then shifting the resulting eigenenergies to reproduce the excitations obtained from TDDFT, and finally transforming the matrix back to the original basis. Then the 4×4 molecular sub-matrix of H_M can be replaced by this corrected matrix to yield the new, corrected model Hamiltonian. This procedure ensures that we only shift the eigenenergies of the molecule (not to be confused with ϵ_i), we do not alter the molecular eigenfunctions and therefore we preserve the original DFT ground-state density, which is expected to be accurate.

III. BUILDING BLOCKS

To understand how the different building blocks of these molecules influence transport properties, we examine transport through a related sequence of molecules, with varying levels of complexity. In this section and

in section IV, the focus is on the qualitative trends contained in the uncorrected DFT-based transmission $T(E)$.

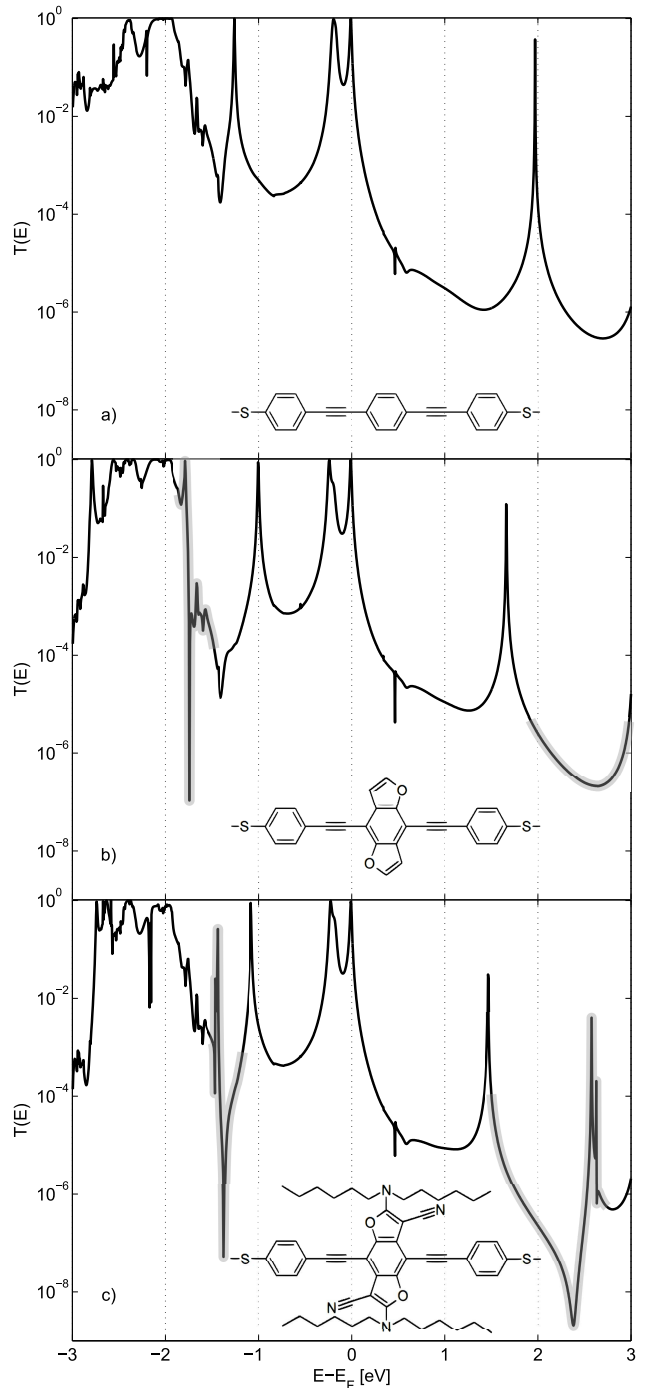


FIG. 4: Zero-bias transmission $T(E)$ against electron energy E for the triple-bonded BDF molecule **3** in stages of building blocks (uncorrected transport curves)

The backbone of molecule **3** of Fig. 1 is the widely-studied OPE system shown in Fig. 4(a) (inset). For this structure, the zero-bias transmission $T(E)$ is shown in Fig. 4(a), which reveals that the Fermi energy ($E_F = 0$ eV) sits close to the HOMO resonance. The

LUMO resonance possesses the shape of a Lorentzian curve, typical of Breit-Wigner transport resonances, whereas the HOMO forms a double-resonance with the close lying HOMO-1.

The next step towards molecule **3** is to replace the central phenyl ring with the BDF core, resulting in the transmission probability shown in (Fig. 4(b)), whose HOMO-2 and the LUMO peaks are shifted closer to the Fermi energy. Around 2.5 eV, the local minimum is also decreased and close to -2 eV, a sharp antiresonance now appears.

In Fig. 4(c), which contains both cyano and amine groups, the transmission probability shows clear examples of Fano resonances,¹⁷ where the line shape consists of a resonant peak followed or preceded by an antiresonance. The addition of these groups lead to the appearance of these two resonances at $E = -1.5$ eV, and at $E = 2$ eV. It is known that Fano resonances arise in molecular wires due to interference effects between a side group and the backbone of the molecule.¹⁷ For molecule **3**, we can conclude that the difuran units with the cyano and amine groups are responsible. These additional groups have caused the Fano resonances to shift, however, the transport behaviour close to the Fermi energy is similar in all three cases shown in Fig. 4.

Further understanding of the transport properties of molecule **3** can be extracted from the orbitals of the isolated molecule. Figure 5 shows the DFT calculated LUMO and LUMO+1 orbitals. The LUMO orbital is heavily weighted along the backbone of the molecule (the HOMO also shows similar behaviour) and this type of orbital typically produces a Breit-Wigner resonance. This contrasts with the LUMO+1 orbital, which is located mainly on the central BDF core. This orbital is responsible for the Fano resonance close to 2 eV in the transmission curve of Fig. 4(c).

IV. SIDE GROUP SUBSTITUTION

The ability to control transport is one of the main aims of single molecule electronics. In the molecular junctions studied in this paper, the HOMO and LUMO resonances are produced by a delocalized orbitals, which are difficult to modify by an external stimulus. However Fano resonances are produced by a localized orbitals, which are more sensitive to environment changes or external fields. Here we carry out a simple theoretical experiment to illustrate how the position of a Fano resonance could be controlled through targeted design.

The furan subunit of **3** can be changed by substituting different atoms in place of the oxygen atoms.³ In what follows, we replace the oxygens by the group-16 atoms, sulphur and selenium, and in each case, find the relaxed geometry of these new, triple-bonded molecules. As an example of the changes in geometry caused by this substitution, the calculated bond lengths between the substituted atom and the backbone are as follows: C-O bond = 1.38 Å, C-S = 1.76 Å and C-Se = 1.9 Å. Figure 6 shows

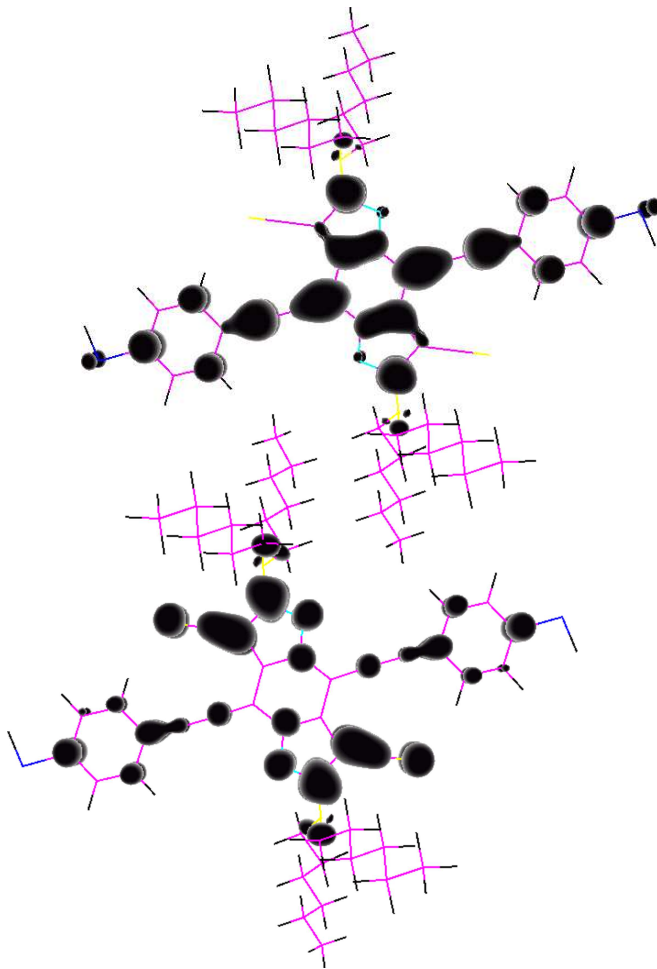


FIG. 5: LUMO (top) and LUMO+1 (bottom) orbitals of the triple-bonded BDF molecule **3**.

the transmission curve through these three molecules, and focuses on the area close to the Fano resonance at 2 eV. As expected, the HOMO resonance is largely unaffected, but we see that both the sulphur and selenium shift the Fano resonance closer to the Fermi energy. For sulphur, the antiresonance and associated resonance are shifted closer to the Fermi energy, with the antiresonance sitting 0.3 eV below that of the oxygen.

V. BDF SERIES OF MOLECULAR WIRES

So far, we have focussed on the uncorrected DFT-based transmission probability. Fig. 7 presents results for the corrected transmission probability of molecule **3** (solid line) and the uncorrected transmission (dotted line). For comparison, the figure also includes results that would be obtained using two alternative correction methods.

The first of the alternative methods is the so-called scissor correction¹¹ and yields the dashed line in Fig. 7. The scissor correction is performed by diagonalizing the molecular sub-matrix of the full Hamiltonian, then shift-

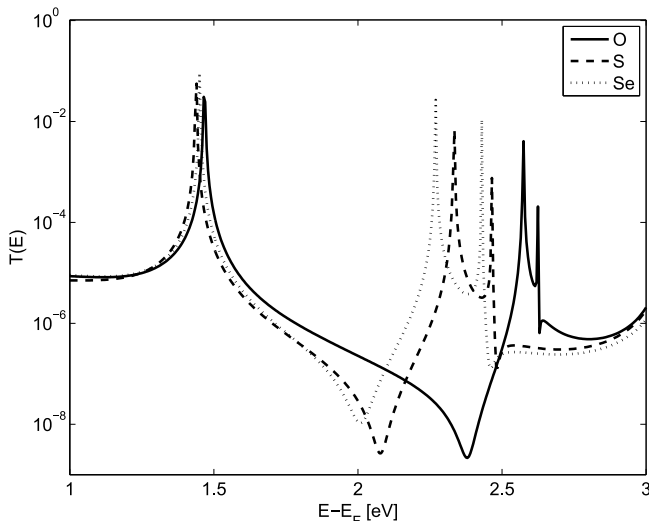


FIG. 6: Transmission in the presence of different substituted atoms (uncorrected transport curves)

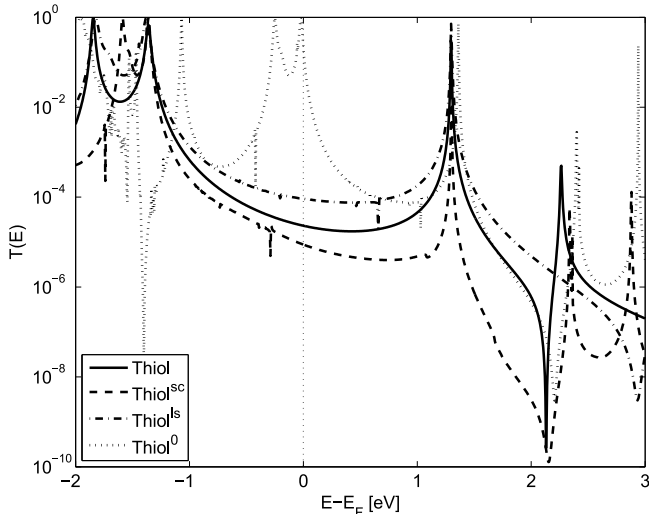


FIG. 7: Zero-bias transmission $T(E)$ for the thiol anchored triple-bonded molecule with the correction in Sec. II (solid line), with the scissor correction (dashed line), with a simple linear scaling of the energy axis (dashed-dotted line) and finally without any correction (dotted line). The conductance values at the Fermi energy are $2.31 \times 10^{-5} G_0$, $8.78 \times 10^{-6} G_0$, $9.20 \times 10^{-5} G_0$ and $2.19 \times 10^{-1} G_0$ respectively.

ing the eigenvalues below and above the Fermi energy such that the new HOMO-LUMO gap matches with the first singlet excitation value of the isolated molecule. Finally the diagonalized matrix is transformed back to the original basis to obtain the corrected full Hamiltonian. The main limitation with this method is that it applies a constant shift to all occupied levels of the discrete spectrum relative to the unoccupied levels and does not allow occupied (or unoccupied) levels to shift relative to each other. In this sense, the method leading to $T_M(E)$ can

be viewed as an extension of the scissor correction.¹¹ The second alternative method (dashed-dotted line in Fig. 7) that one might consider, consists solely of a simple scaling of the energy axis to yield the correct HOMO-LUMO gap. However this has the undesirable effect of increasing the widths of resonances, which would not be consistent with the DFT-computed coupling between the states and the electrodes.

Fig. 7 shows that the correction described in Sec. II produces a curve somewhere in between these two alternatives. Whichever correction method is used, the conductance is decreased by 3-4 orders of magnitude compared to that obtained from the uncorrected $T(E)$. This underlines the importance of correcting for the HOMO-LUMO gap, and the position of the Fermi energy inside the gap.

Next, we examine the effect of the bonding type along the backbone of the molecule by performing calculations on the series of molecules shown in Fig 1. Hereafter we only present corrected results. The single-bonded molecule **1** is the shortest, with a calculated length of 1.52 nm, and the geometry is non-planar, with a twist angle of 44° between the planes of the individual rings. The lengths of the double-bonded and triple-bonded molecules are 1.99 nm and 2.04 nm respectively and both of these molecules are planar. We consider the trans-trans configuration of the double-bonded molecule **2**. (However there is little change in the conducting properties for the trans-cis configuration.) The corrected HOMO-LUMO gaps are presented in Table I.

TABLE I: Theoretical values for the HOMO-LUMO gaps [eV]

	single-bonded BDF	double-bonded BDF	triple-bonded BDF
HOMO-LUMO gap			
by DFT without corrections	2.44	1.27	1.38
1st singlet excitation energy by TDDFT	3.24	2.59	2.80 ¹⁸
ionization potential	6.18	5.95	6.46

In these molecules, the gap is underestimated by pure DFT with GGA by up to 50%, but the general trend does not change. The single-bonded molecule **1** has the largest gap, which is a consequence of its smallest size. It is less obvious why the triple-bonded has the second largest gap, but this can be also understood by considering the effect of bond-length alternation along the π -conjugated backbones,¹⁹ which is somewhat higher in the triple-bonded one than in the double-bonded one due to the stronger bonding.³³

The transmission coefficient $T_M(E)$ of the series of BDF molecules shown in Fig. 1 can be seen in Fig. 8, which shows that the conductance values at the Fermi energy are determined mainly by the position of the

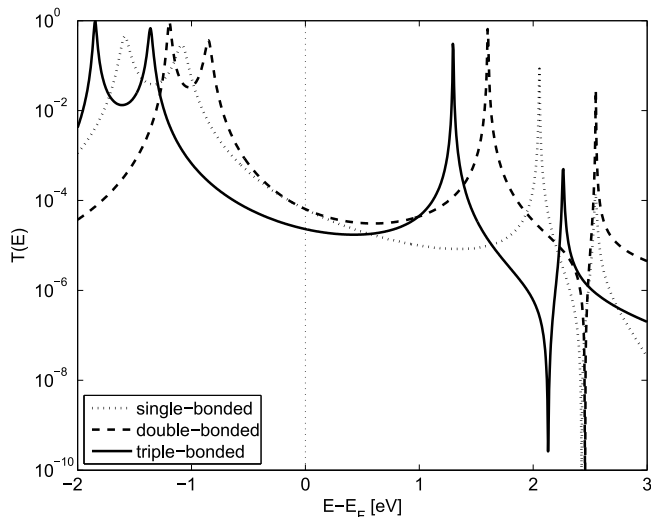


FIG. 8: Zero-bias transmission $T_M(E)$ for single, double and triple-bonded molecules in Fig. 1. At the Fermi energy, $G_{\text{Sb}} = 6.36 \times 10^{-5} G_0$, $G_{\text{Db}} = 6.42 \times 10^{-5} G_0$ and $G_{\text{Tb}} = 2.31 \times 10^{-5} G_0$.

HOMO peak. Despite having the largest HOMO-LUMO gap, and the twisted conformation,²⁰ the single-bonded molecule comes second after the double-bonded one. Without any corrections, the conductance values would be higher by four orders of magnitude, with the single-bonded having the lowest conductance: $G_{\text{Sb}} = 1.86 \times 10^{-1} G_0$, $G_{\text{Db}} = 4.52 \times 10^{-1} G_0$ and $G_{\text{Tb}} = 2.19 \times 10^{-1} G_0$.

VI. DIFFERENT ANCHOR GROUPS

We now study the effect of varying the type of anchor groups of the triple-bonded BDF shown at the bottom of Fig. 1 by computing the transmission probabilities of the molecules shown in Fig. 9, obtained by replacing the

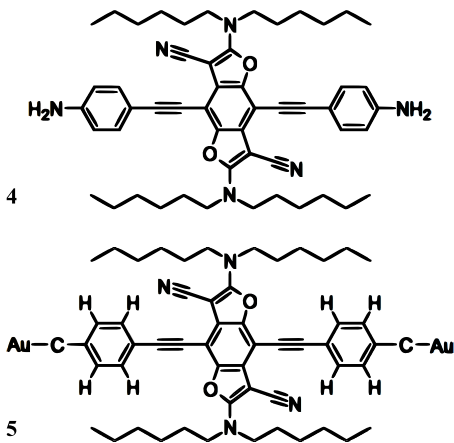


FIG. 9: Structure of the triple-bonded BDF molecules with amine anchors and direct C-Au bonds

thiol groups by amine groups and by direct Au-C bonds. In the former case, the bonding sulphur atom is replaced by the NH_2 group, and in the latter case, by the CH_2 group. Amines have previously been shown to form more stable junctions, and a direct gold-carbon bond is also believed to form a very strong connection to the leads.²¹ For molecules **4** and **5**, we carried out the same geometry and transport calculations with corrections, and the results are shown in Fig. 10. Not surprisingly, the HOMO-

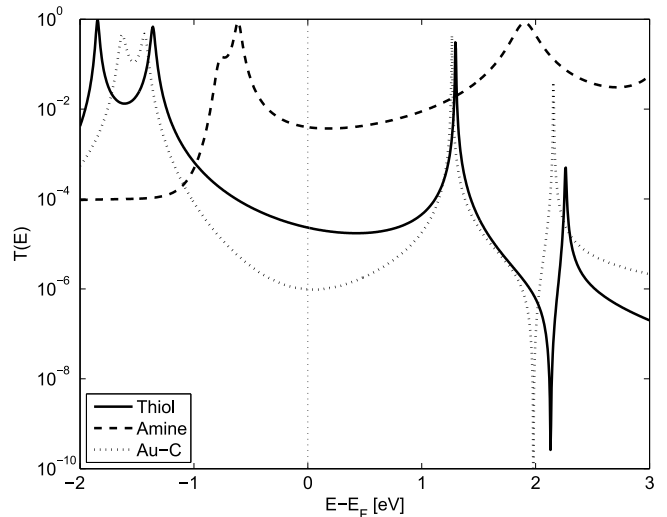


FIG. 10: Zero-bias transmission $T_M(E)$ for the thiol, amine and Au-C anchored triple-bonded molecules. At the Fermi energy, $G_{\text{thiol}} = 2.31 \times 10^{-5} G_0$, $G_{\text{amine}} = 3.96 \times 10^{-3} G_0$ and $G_{\text{Au-C}} = 9.73 \times 10^{-7} G_0$.

LUMO gap of all these molecules are very close to each other: 2.80 eV for the thiolated one, 2.72 eV for the amine anchored molecule and 2.76 eV for the Au-C type. In all the cases, the Fermi energy is close to the minimum of $T_M(E)$ in the HOMO-LUMO gap, which yields the estimated conductance values shown in the figure caption. There is a significant difference in the conductance between the studied molecules, which can be attributed to the following factors.

Firstly, the low conductance of the Au-C system is surprising, since it has the strongest coupling to the leads with a bond length of 1.96 Å.²¹ We note however, that the corrections are less reliable in this particular case because of the uncertainty in the Fermi energy. This is caused by the fact that the dangling carbon bonds, which form strong Au-C bonds in the junction, are saturated with hydrogens in the calculation of the ionization potential. In the junction, the molecule can get charged, which renders the HOMO level somewhat ambiguous.

Secondly, in the case of the thiol, a relatively high conductance is expected as reported in various theoretical and experimental works with thiol and conjugated systems.^{22,23} The high conductance is usually explained with strong thiol-gold coupling, since the sulphur atom tends to bind to multiple gold atoms preferentially in

hollow position. However in the presented geometry the sulphur atoms binds to a single apex gold atom, thus resulting rather an estimated minimum for the conductance. The apex bonding geometry also accounts for the narrow resonance peaks.

Thirdly, since amine has a selective binding preference to apex gold atoms with special bonding geometry due to the steric hinderance of the two hydrogen atoms,¹⁰ we constructed the anchor geometry from the work of Hong et al.²² The Au-N bond length between the apex gold atom and the amine group was 2.33 Å. The calculated transmission probability, in agreement with previous studies, shows wide resonance peaks and relatively large overall conductance, that is attributed to the strong Au-N bond. The results suggest that in a fully stretched configuration of BDF, the amine anchor's conductance is the least sensitive to the change in the Fermi energy.

VII. THERMOELECTRIC PROPERTIES

We now turn to the room-temperature thermoelectric properties of the above molecules, which can be obtained from weighted integrals of $T(E)$ around the Fermi energy.²⁴ The resulting electrical conductance G , the thermal conductance κ and the thermopower S are shown in Table II. The thermopower or Seebeck coefficient S of a

TABLE II: Conductance (G), thermal conductance (κ) and thermopower (S) for the single-, double- and triple-bonded thiolated molecules, and the amine and Au-C anchored molecules at room temperature (300K)

	G [nS]; [G_0]	κ [keV/s/K]	S [μ V/K]
1 - Thiol Sb	4.99; 6.44×10^{-5}	233	21.5
2 - Thiol Db	5.05; 6.51×10^{-5}	238	19.7
3 - Thiol Tb	1.80; 2.32×10^{-5}	83.3	9.62
4 - Amine Tb	309; 3.99×10^{-3}	14489	6.46
5 - Au-C Tb	0.076; 9.82×10^{-7}	3.58	2.61

material or of a nanojunction is defined as

$$S = -\frac{\Delta V}{\Delta T},$$

where ΔV is the voltage difference between the two ends of the junction when a temperature difference ΔT is established between them. This quantity controls the direct conversion of heat into electric energy at a molecular scale. If $T(E)$ varies only slowly with energy on the scale of $k_B T$, where T is the temperature, k_B Boltzmann's constant, then the exact expression²⁴ for S simplifies to

$$S = -\frac{\pi^2 k_B^2 T}{3e} \frac{\partial \ln T(E)}{\partial E}$$

evaluated at $E = E_F$, and e is the magnitude of the electronic charge. For example, this means that if the

LUMO resonance is closer to the Fermi energy than the HOMO, such that the slope of $\ln T(E)$ at $E = E_F$ is positive, then S will be negative.

Table II shows that the thermopower of molecules **1** and **2** are comparable with the highest values of S measured to date for single molecules. For example, recently-measured values of S at room temperature include 8.7, 12.9 and 14.2 μ V/K for 1,4-benzenedithiol (BDT), 4,4'-dibenzenedithiol, and 4,4''-tribenzenedithiol in contact with gold respectively,²⁵ -1.3 to 8.3 μ V/K for the benzene-based series of benzene-dithiol (BDT), 2,5-dimethyl-1,4-benzenedithiol (BDT2Me), 2,3,5,6-tetrachloro-1,4-benzenedithiol (BDT4Cl), 2,3,5,6-tetrafluoro-1,4-benzenedithiol (BDT4F) and BDCN,^{26,27} 7.7 to 15.9 μ V/K for the series BDT, DBDT, TBDT and DMTBDT,²⁸ -12.3 to 13.0 for a series of amine-Au and pyridine-Au linked molecules.²⁹

The thermopower of molecules **1** and **2** exceed all of these values. Only fullerene-based single-molecule junctions³⁰⁻³² with S ranging from -8.9 to -33.1 μ V/K have been measured to have higher values.

VIII. CONCLUSIONS

The conductance of a series of short molecular wires containing BDF cores has been studied to assess their performance as components in molecular devices. The appearance of Fano resonances has been investigated and we have demonstrated that the positions of Fano resonance can be controlled via the electronegativity of the atoms of the side groups attached to the backbone. We have also made a comparison between the single-, double- and triple-bonded BDF molecules with thiol anchor groups contacting apex gold atoms, followed by an extended comparison with two other anchor groups including amine and direct Au-C bonding.

The room-temperature thermoelectric parameters of the given molecules have been evaluated. Table II shows that the largest thermopower is predicted for molecule **1**. This value is comparable with the highest measured values for single-molecule thermopower reported to date. The thermopower is approximately proportional to the slope of $\ln T_M(E)$ at $E = E_F$ and therefore the high value of S for molecule **1** is a reflection of the high slope of the corresponding curve in Fig 8. This high slope is a consequence of the suppression of the LUMO resonance for this molecule, compared with **2** and **3**. For all molecules considered, the Fano resonances are not located close to E_F and play only a minor role in determining thermoelectric coefficients.

Acknowledgments

The authors wish to acknowledge support from the Marie-Curie ITNs MOLESCO and NanoCTM and from EPSRC. Special thanks to Silvio Decurtins, Shi-Xia Liu

and Toni Frölich who provided us with valuable discussions and experimental data.

-
- * Electronic address: c.lambert@lancaster.ac.uk
- ¹ C. Yi, C. Blum, M. Lehmann, S. Keller, S.-X. Liu, G. Frei, A. Neels, J. Hauser, S. Schürch, and S. Decurtins, *The Journal of Organic Chemistry* **75**, 3350 (2010).
 - ² H. Tsuji, C. Mitsui, L. Iles, Y. Sato, and E. Nakamura, *Journal of the American Chemical Society* **129**, 11902 (2007).
 - ³ N. Hayashi, Y. Saito, H. Higuchi, and K. Suzuki, *The Journal of Physical Chemistry A* **113**, 5342 (2009).
 - ⁴ I. Baraldi, E. Benassi, S. Ciorba, M. Sindler-Kulyk, I. Skoric, and A. Spalletti, *Chemical Physics* **361**, 61 (2009), ISSN 0301-0104.
 - ⁵ C. M. Finch, V. M. García-Suárez, and C. J. Lambert, *Phys. Rev. B* **79**, 033405 (2009).
 - ⁶ A. R. Rocha, V. M. García-Suárez, S. Bailey, C. Lambert, J. Ferrer, and S. Sanvito, *Phys. Rev. B* **73**, 085414 (2006).
 - ⁷ A. R. Rocha, V. M. García-Suárez, S. Bailey, C. Lambert, J. Ferrer, and S. Sanvito, *Nature Mat.* **4**, 335 (2005).
 - ⁸ J. M. Soler, E. Artacho, J. D. Gale, A. García, J. Junquera, P. Ordejón, and D. Sánchez-Portal, *Journal of Physics: Condensed Matter* **14**, 2745 (2002).
 - ⁹ J. P. Perdew, K. Burke, and M. Ernzerhof, *Phys. Rev. Lett.* **77**, 3865 (1996).
 - ¹⁰ S. Y. Quek, L. Venkataraman, H. J. Choi, S. G. Louie, M. S. Hybertsen, and J. Neaton, *Nano Letters* **7**, 3477 (2007).
 - ¹¹ V. M. García-Suárez and C. J. Lambert, *New J. Phys.* **13**, 053026 (2011).
 - ¹² R. E. Sparks, V. M. García-Suárez, D. Z. Manrique, and C. J. Lambert, *Phys. Rev. B* **83**, 075437 (2011).
 - ¹³ M. Valiev, E. Bylaska, N. Govind, K. Kowalski, T. Straatsma, H. Van Dam, D. Wang, J. Nieplocha, E. Apra, T. Windus, et al., *Computer Phys. Commun.* **181**, 1477 (2010), ISSN 0010-4655.
 - ¹⁴ A. D. Becke, *J. Chem. Phys.* **98**, 5648 (1993).
 - ¹⁵ P. K. Nayak and N. Periasamy, *Organic Electronics* **10**, 1396 (2009).
 - ¹⁶ P. A. Tipler and R. A. Llewellyn, *Modern Physics* (W.H. Freeman, 1999), 3rd ed.
 - ¹⁷ T. A. Papadopoulos, I. M. Grace, and C. J. Lambert, *Phys. Rev. B* **74**, 193306 (2006).
 - ¹⁸ S.-X. Liu, unpublished: The optical HOMO-LUMO gap of the thiolated triple-bonded BDF has been determined from the intersection of the absorption and emission spectra in CH₂Cl₂ to be 2.53 eV.
 - ¹⁹ J. G. Kushmerick, D. B. Holt, S. K. Pollack, M. A. Ratner, J. C. Yang, T. L. Schull, J. Naciri, M. H. Moore, and R. Shashidhar, *Journal of the American Chemical Society* **124**, 10654 (2002).
 - ²⁰ L. Venkataraman, J. E. Klare, C. Nuckolls, M. S. Hybertsen, and M. L. Steigerwald, *Nature* **442**, 904 (2006).
 - ²¹ Z.-L. Cheng, R. Skouta, H. Vazquez, J. Widawsky, S. Schneebeli, W. Chen, M. Hybertsen, R. Breslow, and L. Venkataraman, *Nat Nano* **6**, 353 (2011).
 - ²² W. Hong, D. Z. Manrique, P. Moreno-García, M. Gulcur, A. Mishchenko, C. J. Lambert, M. R. Bryce, and T. Wandlowski, *J. Am. Chem. Soc.* **134**, 2292 (2012).
 - ²³ T. Frölich, unpublished: The conductance of the thiolated triple-bonded BDF has been determined using break junction measurements to be $2.7 \times 10^{-4} G_0$.
 - ²⁴ C. M. Finch, V. M. García-Suárez, and C. J. Lambert, *Phys. Rev. B* **79**, 033405 (2009).
 - ²⁵ P. Reddy, S.-Y. Jang, R. Segalman, and A. Majumdar, *Science* **315**, 1568 (2007).
 - ²⁶ J. A. Malen, S. K. Yee, A. Majumdar, and R. A. Segalman, *Chem. Phys. Lett.* **491**, 109 (2010).
 - ²⁷ K. Baheti, J. A. Malen, P. Doak, P. Reddy, S. Y. Jang, T. D. Tilley, A. Majumdar, and R. A. Segalman, *Nano Lett.* **8**, 715 (2008).
 - ²⁸ J. A. Malen, P. Doak, K. Baheti, T. D. Tilley, A. Majumdar, and R. A. Segalman, *Nano Lett.* **9**, 3406 (2009).
 - ²⁹ J. R. Widawsky, P. Darancet, J. B. Neaton, and L. Venkataraman, *Nano Lett.* **12**, 354 (2012).
 - ³⁰ S. K. Yee, J. A. Malen, A. Majumdar, and R. Segalman, *Nano Lett.* **11**, 4089 (2011).
 - ³¹ S. Yee, J. Malen, P. Reddy, R. Segalman, and A. Majumdar, *Proc. of the 14th Int. Heat Transfer Conf., IHTC14-22690*, Washington, DC, USA (2010).
 - ³² C. Evangeli, K. Gillemot, E. Leary, M. T. González, G. Rubio-Bollinger, C. J. Lambert, and N. Agraït, accepted to *Nanoletters* (2013).
 - ³³ Note that the gas phase TDDFT calculations cannot include the effect of the image charges in the leads, which tends to decrease the value of the HOMO-LUMO gap.